Ag$_n^+$ quantum dots obtained via in situ photodeposition method as photocatalytic CO$_2$ reduction cocatalyst: Borrowing redox conversion between Ag$^+$ and Ag^0

Hailong Zheng[a], Zaiyong Jiang[b], Huishan Zhai[a], Zhaoke Zheng[a,*], Peng Wang[a], Zeyan Wang[a], Yuanyuan Liu[a], Xiaoyan Qin[a], Xiaoyang Zhang[a], Baibiao Huang[a,*]

[a] *State Key Lab of Crystal Materials, Shandong University, Jinan 250100, PR China*
[b] *State Key Laboratory of Biobased Material and Green Papermaking, Qilu University of Technology, Shandong Academy of Sciences, Jinan 250353, PR China*

ARTICLE INFO

ABSTRACT

Ag$_n^+$-loaded TiO$_2$ (Ag$_n^+$/TiO$_2$) nanocomposites were prepared by an in situ photodeposition method. There is no sacrificial agent during the loading procedure, and the photo-reduction process is always accompanied by a photo-oxidation process, resulting in the simultaneous presence of Ag^0 and Ag$^+$. Surprisingly, the obtained Ag$_n^+$ clusters can be considered as quantum dots with an average size of 2.75 nm, and this quantum size for noble metal is very difficult to get by conventional photodeposition method. Furthermore, we can adjust the ratio of Ag^0 and Ag$^+$ to achieve dynamic balance by changing the processing temperature (60 °C - yellow to 180 °C - violet black). The results indicate that the ratio of Ag^0 and Ag$^+$ is a key factor for the photocatalytic efficiency.

1. Introduction

Due to the large global consumption of fossil fuels and the enhancement of atmospheric carbon dioxide, the feasible photocatalytic reduction of CO$_2$ has attracted increasing attention [1–3], owing to that the artificial photosynthesis can transform the CO$_2$ into usable fuels to overcome the greenhouse effect as much as possible [4–7]. Up to now, various smiconductor photocatalysts, such as CdS [8], TiO$_2$ [9], Bi$_2$WO$_6$ [10], SrTiO$_3$ [11], and MOF compounds [12,13] et al., have been reported in application of CO$_2$ reduction. Among them, TiO$_2$ is considered to be a suitable photocatalyst for CO$_2$ photoreduction because of its high chemical stability, nontoxic, thermally stable and environmentally friendly, which is important for CO$_2$ photoconversion in an aqueous environment [14–18]. There are many methods have been reported so far to improve the CO$_2$ photoconversion activity based on TiO$_2$, such as doping of elements [19,20], recombination of semiconductors [21,22], loading of cocatalysts [23–27], regulation of crystal-facet [28,29], and so on. However, the efficiency is still low, which could not meet practical application requirements.

Generally, the cocatalysts could significantly improve the photocatalytic CO$_2$ reduction efficiency via providing more active sites and suppressing the recombination of photogenerated carriers. The typical cocatalysts mainly include Pt [30], Ag [31], Pd [32], et al. Among

them, Ag has attracted widespread attentions because the cost of which is much lower. Moreover, Ag as a cocatalyst has many fascinating properties, which is not inferior to other noble metals on promoting the activity of TiO$_2$. For example, Ag/(anatase/brookite) TiO$_2$ microspheres shows remarkable enhanced CO$_2$ reduction efficiency, which demonstrated that Ag serves as a sink to accumulate photogenerated electrons by the Schottky barrier at the Ag–TiO$_2$ interface [33]. Peng et al. proved that the different exposed crystal facets of brookite nanocubes for Ag loading and the size of Ag nanoparticles can significantly affect the activity and selectivity of CO$_2$ photoreduction to CO/CH$_4$ [34]. As far as we know, the studies of Ag as the cocatalyst on photocatalytic CO$_2$ reduction are mainly focused on Ag nanoparticles (NPs). However, the Ag clusters with smaller size is rarely reported. Therefore, it will be a very meaningful work to assemble Ag clusters as a cocatalyst, in which to explore the effect of Ag clusters toward CO$_2$ photoconversion activity. At the same time, a large number of reports indicate that when Ag@TiO$_2$ composites are synthesized by the in situ photodeposition method, almost all of the Ag NPs are loaded on the low-active {101} reduction facet not on the high-active {001} oxidation facet [35,36]. Therefore, it is worth attemptting to load Ag on the high-active oxidation plane.

Herein, Ag clusters was successfully immobilized on the {001} oxidation plane of TiO$_2$ nanosheets via an in situ photodeposition
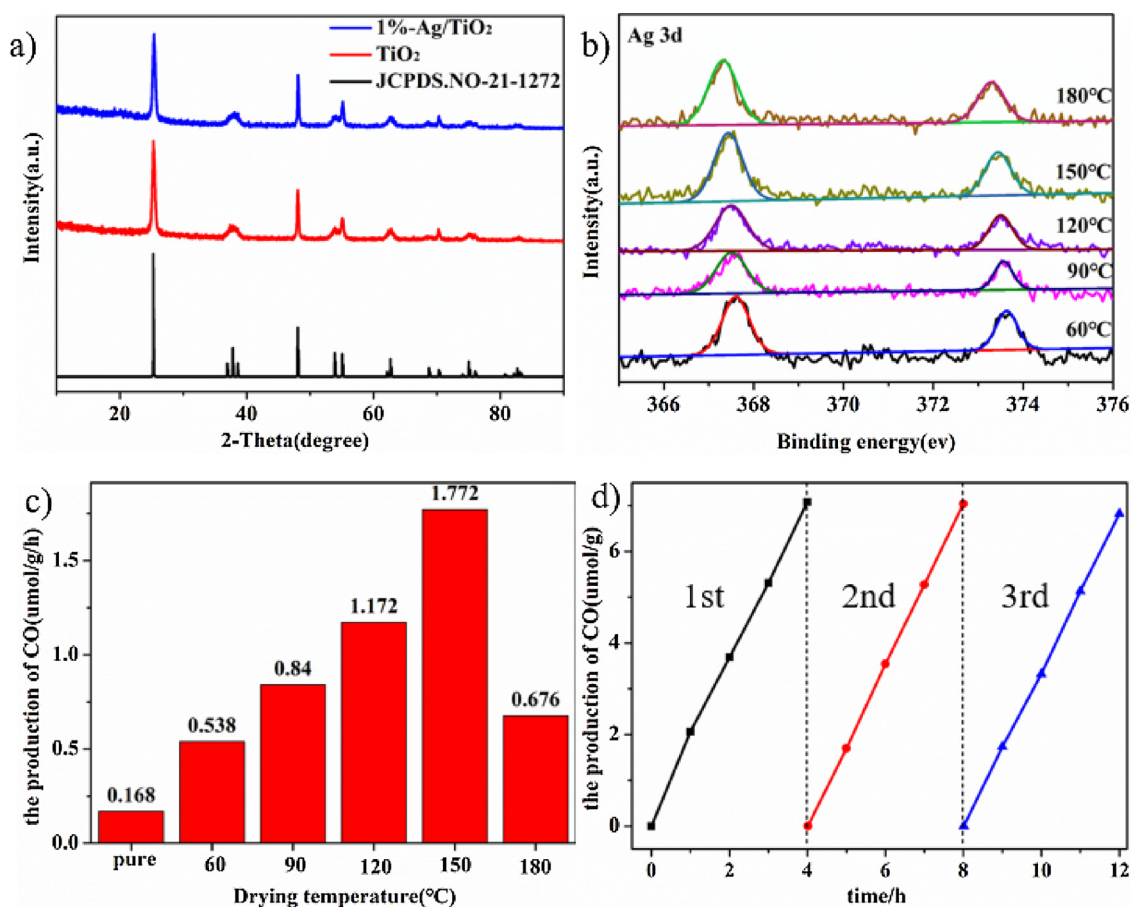
Fig. 1. (a) XRD patterns of all samples (b) High-resolution XPS spectra of the Ag_n^+/TiO_2 samples processed with different temperature (c) CO yield of the Ag_n^+/TiO_2 samples processed with different temperature under UV–vis light irradiation. (d) Repeated photocatalytic CO_2 reduction activity in H_2O with the Ag_n^+/TiO_2 sample processed at 150 °C as photocatalyst.

method without any sacrificial agent. Certainly, oxidation may occur in Ag clusters on the high-active oxidation facet, hence Ag_n^+ clusters was assembled to transfer holes. As expected, Ag_n^+ clusters loaded on TiO_2 exhibits much better CO_2 photoconversion performance compared to that of pure TiO_2, which is attributed to the Ag_n^+ clusters have significant acceleration to TiO_2 on separating the photogenerated electron-hole pairs.

2. Experimental section

2.1. Materials

Ti(OBu)$_4$, hydrofluoric acid solution (40%), and AgNO$_3$ were provided from the Sinopharm Chemical Reagent Corporation (Shanghai, China). All materials, which were analytical grade, were used without further purification in this study.

2.1.1. Synthesis of TiO$_2$ nanosheets
TiO$_2$ nanosheets with highly reactive {001} facets were synthesized as follows: Ti(OBu)$_4$ (15 mL) was mixed with hydrofluoric acid solution (3 mL, 40%) under vigorous stirring. The resulting solution was stirred for 30 min, transferred into a dried Teflon autoclave, which was kept at 200 °C for 24 h. After being cooled to room temperature and washed by water and ethanol, the white precipitate was dried at 60 °C overnight.

2.2. Preparation of the Ag_n^+/TiO_2 nanocomposite

AgNO$_3$ aqueous solution (0.1 mL, 0.185 M) was injected into the TiO$_2$ suspension aqueous solution (0.4 g, 100 ml). After stirring for

10 min, take the solution under the photoreactor and irradiated for 30 min to make Ag_n^+ cluster grow on the TiO$_2$ surface. Fluoride ions strongly adsorb silver ions, and there is no sacrificial agent during the loading process, then the reduction process is accompanied by an oxidation process, as shown in Fig.S1. After being filtered and washed by water and ethanol, the precipitate was dried at different temperatures (60 °C, 90 °C, 120 °C, 150 °C, 180 °C) for 5 h, as shown in Fig.S2. The Ag/TiO$_2$ samples after Fluoride removal or with the sacrificial agent were also prepared and characterized by us. As shown in Fig.S3, almost all of the Ag NPs are loaded on the low-active {101} reduction facet and the size of the Ag NPs is bigger.

2.3. Characterization

X-ray powder diffraction (XRD) pattern was measured on a Bruker AXS D8 diffractometer with Cu Kα radiation (λ = 1.5406 Å). UV–vis diffuse reflectance spectroscopy (DRS) absorption spectra (BaSO$_4$ was used as a reference) were investigated by Shimadzu UV 2550 spectrophotometer. The morphologies of the samples were measured by scanning electron microscopy (SEM, Hitachi S-4800) and transmission electron microscopy (TEM, JEOL JEM-2100 F). X-ray photoelectron spectroscopy (XPS) spectra were recorded on Thermo Fisher Scientific Escalab 250 spectrometer equipped with Al Kα X-rays, and the binding energies were calibrated by the C 1s peak (284.6 eV). The photoluminescence (PL) was analyzed on a Hitachi F-4500 fluorescence spectrophotometer with the excitation wavelength of 320 nm. The time resolved fluorescence spectra were recorded at 460 nm using a 320 nm excitation by Edinburgh FLS920 PL, decay curves were fitted by using a biexponential decay function to obtain deconvolution of the instrument

response function.

2.4. Photocatalytic CO₂ reduction evaluation

The process of photocatalytic reduction of CO_2 is follows: 0.1 g Ag_n^+/TiO_2 sample was mixed into 100 mL water with vigorous stirring, and high purity CO_2 gas was continuously bubbled through the solution for 1 h before the lamp turn on. A 300 W Xe arc lamp (PLS-SXE300, Beijing Trusttech Co., Ltd.) was used as the light source. The temperature of reactor of photocatalytic CO_2 reduction was controlled at 15 ℃, to increase the solubility of CO_2 via using cooling water circulation. At the given time interval, the gas was withdrawn and the product was monitored by GC-7920 gas chromatograph (FID detector, YQ1229 column).

3. Results and discussion

In order to systematically investigate the results, the crystalline structures of the as-prepared samples were firstly characterized via powder X-ray diffraction (XRD). As shown in Fig. 1a, the diffraction peaks for all samples can be perfectly identified as the anatase TiO_2 structure (JCPDS no. 21-1272), which means the crystal structure of TiO_2 is not changing after loading of Ag. Besides, there are no diffraction peaks of Ag^0 or Ag^+ in the 1%-Ag/TiO_2 samples, which indicate that the detection sensitivity is insufficient to form the peak with too little content.

To identify the valence states of the Ag ions and the chemical composition of the deposited samples, all the products processed with different temperature were analyzed by XPS. The high resolution XPS spectra of the Ag 3d binding energy regions are shown in Fig. 2b. We can see two distinct peaks occur at 367.5~368.2 eV and 373.5~374.2 eV. As we know, the peaks located at 367.5 and 373.5 eV can be attributed to the characteristic orbital splitting of the Ag 3d$^{5/2}$ and Ag 3d$^{3/2}$ which are features of the Ag^+. And two peaks located at 368.2 and 374.2 eV can be ascribed to the characteristic orbital splitting of the Ag 3d$^{5/2}$ and Ag 3d$^{3/2}$, which are features of the Ag^0 [37–39]. Thus the silver ions in our sample exist in a mixed state. Meanwhile, as increasing the processing temperature, the characteristic peaks of the 3d orbit of silver shift to the lower energy state in a regular manner, which means that as the processing temperature increases, the positive valence of silver increases. Therefore, the ratio of Ag^0 and Ag^+ can be controlled by varying the processing temperature.

To study the optical properties of the samples, the UV–vis absorption spectra were measured. As shown in Fig.S4, all the samples exhibit strong absorption in the range below 390 nm. It is attributed to the characteristic absorption of TiO_2 from band–band electron transition. Comparing with pure TiO_2, all the samples processed with different temperatures exhibit broad absorption in the visible region due to the SPR effect of Ag dots and the surface plasmon absorption gives the valid

evidence that Ag indeed exist in the samples [40].

The ratio of Ag^0 and Ag^+ was optimized by detecting the yield of CO (Fig. 1c), a series of as-prepared samples were prepared and noted as 60 ℃, 90 ℃, 120 ℃, 150 ℃ and 180 ℃ based on different processing temperatures. It is observed that pristine TiO_2 has a poor reaction rate constant of 0.168 μmol/g/h. After loading of Ag_n^+, the yield of CO shows different extent of improvement. Particularly, the sample processed at 150℃ exhibits the highest activity of CO_2 photoconversion and reaction rate is even reaching up to 1.772 μmol/g/h, which is about 10 times higher than that of pure TiO_2. It can be seen the different ratio of Ag^0 and Ag^+ in the Ag_n^+ cluster has a great influence on reactivity of CO_2 reduction.

In order to confirm the stability of the obtained Ag_n^+/TiO_2 samples, the photocatalytic CO_2 reduction reaction of the samples processed at 150 ℃ was circularly carried out for three times. After each cycle, the sample was collected, washed, dried and then continued to perform photocatalytic CO_2 conversion in water solution. The result of the cycle experiment was shown in Fig. 1d, implying that the samples processed at 150 ℃ have carried out a relatively excellent recyclability under ultraviolet visible (UV–vis) light irradiation. And the sample after cycle experiment was characterized by TEM and XPS (Fig.S5). Compared with the initial Ag_n^+/TiO_2 TEM patterns and XPS spectra, there is no change after three cycles, indicating that Ag_n^+/TiO_2 samples is very stable and really have industrial application prospects.

The effective generation and instant separation of photo-excited charge carriers are crucial for the photocatalytic reactions [41]. The room-temperature PL and TRPL (the time resolved fluorescence) spectra were measured to characterize the recombination rate and lifetime of photo-generated electrons and holes [42,43]. As shown in Fig. 2a, the positions of the emission peaks of Ag_n^+/TiO_2 samples were similar compared with that of TiO_2, but all intensity decreased and the sample processed at 150℃ exhibited the lowest intensity. This result suggests that the samples processed at 150℃ has the lowest recombination rate of photo-generated charge carriers compared with pure TiO_2 and other Ag_n^+/TiO_2 composites [44–46]. Moreover, the TRPL decay spectra of the pure TiO_2 and the Ag_n^+/TiO_2 sample processed at 150 ℃ is shown in Fig. 2b, the average lifetime is calculated using the following relation: $\tau av = a1\tau1 + a2\tau2 + a3\tau3$, ($\tau1,\tau2$ and $\tau3$ are the lifetime, a1, a2 and a3 are normalized pre-exponential factors) [47]. The average life times of pure TiO_2 and the Ag_n^+/TiO_2 sample processed at 150℃ are evaluated to be 2.07 and 4.33 ns, respectively. The Ag_n^+/TiO_2 sample processed at 150 ℃ has the slower decay rate. A longer lifetime is equivalent to decreasing the recombination rate of photogenerated charge carrier, leading to a more efficient electronhole separation [48], which is very conducive to photocatalytic activity. In short, the slower recombination rate in the Ag_n^+/TiO_2 composites implies the introductions of Ag_n^+ nanoparticles can significantly suppress the recombination of photogenerated charge carriers than those in the pristine TiO_2. This result is consistent with that Ag_n^+/TiO_2
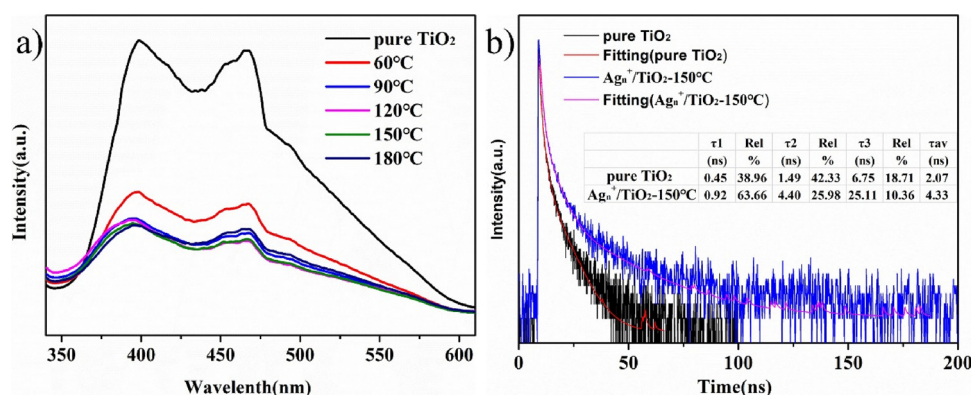

Fig. 2. (a) PL spectra of all samples, (b) TRPL decay spectra of the pure TiO_2 and the Ag_n^+/TiO_2 sample processed at 150 ℃.
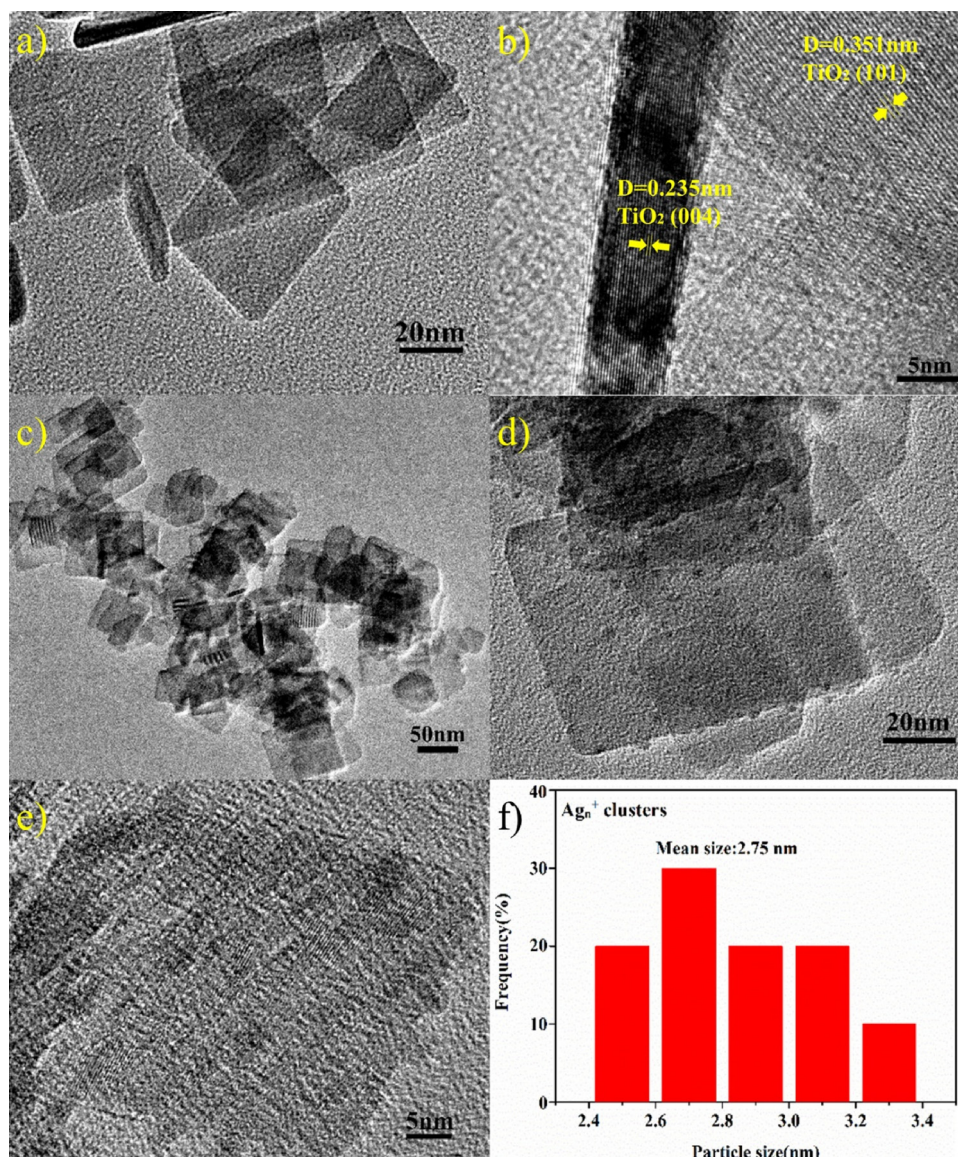
Fig. 3. TEM images of TiO_2 (a, b) and the Ag_n^+/TiO_2 sample processed at 150 °C (c, d, e, f).

composites exhibit much higher photocatalytic CO_2 reduction performance.

The morphologies of pure TiO_2 and Ag_n^+/TiO_2 samples were investigated by scanning electron microscopy (SEM). As shown in Fig.S6 and Fig.S7, the morphologies before and after the deposition of Ag_n^+ are almost identical. And then, Fig.S8 exhibits the energy dispersive X-ray spectrum (EDS) information of the Ag_n^+/TiO_2 sample, further confirming the presence of Ag elements. The corresponding EDS mappings of elemental O, Ti and Ag of 150 °C-Ag_n^+/TiO_2 are shown in Fig.S9. This result proves that Ag elements are uniformly loaded on the surface of TiO_2. To further analyze the surface morphologies, the pristine TiO_2 and 150 °C-Ag_n^+/TiO_2 were chosen to investigate the surface state using transmission electron microscope (TEM). It is observed that the average sizes of TiO_2 nanosheets are about 30 nm (width), 50 nm (length) and 4 nm (thickness), respectively (Fig. 3a). The insert image of Fig. 3b showed the measured lattice spacing is ca. 0.351 nm on the large plane, which is matched well with the (101) planes of pristine anatase TiO_2, the measured lattice spacing is ca. 0.235 nm on the side plane, which is matched well with the (004) planes of pristine anatase TiO_2. It is worth mentioning that high exposed face of pristine TiO_2 we synthesized was {001} crystal face. After

the deposition of Ag_n^+, the sizes of TiO_2 nanosheets have no obvious change (Fig. 3c-f) and the Ag_n^+ nanoparticles uniformly disperse on the TiO_2 {001} crystal face, in which their average particle size is quantum dots level, ca. 2.75 nm. Such a small size and such a uniform distribution are also important reasons for high activity of Ag_n^+/TiO_2.

We know that the photocatalytic properties largely depend on the surface atom arrangement and synergy of different crystal planes [49,50]. Due to the atom arrangement characteristics on crystal planes, different crystal facets have different surface energy levels of the conduction band and valence band [51,52]. For anatase TiO_2, theoretical calculations and extensive experimental studies have shown that the oxidation sites are on the {001} plane and the reduction sites are on the {101} plane [53,54]. The results of TEM images, EDS mappings and High-resolution XPS spectra fully prove that we have successfully loaded Ag_n^+ nanoparticles on the highly exposed 85% and highly active oxide surface {001} plane. Based on the experimental results, Fig. 4 presents a possible mechanism for photocatalytic CO_2 reactions. Under UV–vis light irradiation, TiO_2 is excited to generate photo-generated electrons (e^-) and holes (h^+). On the reduction plane, single silver captures electrons and acts as a reactive site. On the highly active oxide plane, Ag^0 in the Ag_n^+ cluster rapidly captures photogenerated holes to
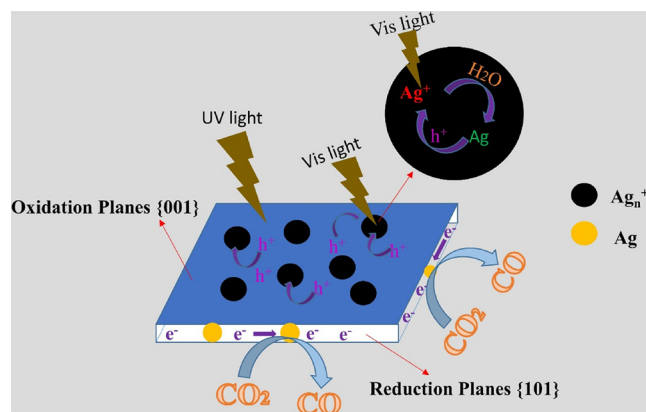
Fig. 4. The Schematic illustration of photocatalytic CO_2 reduction into CO of Ag_n^+/TiO_2 product.

transform into Ag^+. The CB position of Ag^+ is approximately 0.19 eV and is excited by visible light to generate Ag^0 [55,56]. Compared with the initial Ag_n^+/TiO_2 TEM patterns and XPS spectra, there is no change of the Ag_n^+/TiO_2 sample after three cycles, indicating that Ag_n^+/TiO_2 sample is very stable. Briefly, under the action of visible light, Ag_n^+ cluster forms a cycle of Ag^0 and Ag^+ in the aqueous phase by trapping the photogenerated holes of TiO_2. Throughout the process, silver acts as a cocatalyst and hole-electron trap to induce efficient separation of photogenerated electrons and holes, thereby enhancing photocatalytic carbon dioxide reduction activity.

4. In summary

Ag_n^+ clusters as a hole-cocatalyst was successfully immobilized on the surface of TiO_2 nanosheets by an in situ photodeposition method without any sacrificial agent. As expected, Ag_n^+/TiO_2 composite photocatalyst exhibits much better CO_2 photoconversion performance compared to that of pure TiO_2. The reason was attributed to the introduction of Ag_n^+ clusters, which can significantly improve the separation efficiency of the photogenerated electron-hole pairs. In the Ag_n^+ clusters, Ag^0 can be oxidized by holes to transform into Ag^+, subsequently, the Ag^+ could reconvert into Ag^0 clusters under the visible light irradiation. Finally, the ratio of Ag^0 and Ag^+ can be adjusted by changing the processing temperature (60 °C–180 °C), and a suitable ratio of Ag^0 and Ag^+ is the key to the catalytic efficiency.

Appendix A. Supplementary data

Supplementary material related to this article can be found, in the online version, at doi:https://doi.org/10.1016/j.apcatb.2018.10.053.

References

[1] G.A. Ozin, Energy Environ. Sci. 8 (2015) 1682–1684.
[2] K.F. Li, X.Q. An, K.H. Park, M. Khraisheh, J. Tang, Catal. Today 224 (2014) 3–12.
[3] S.N. Habisreutinger, L. Schmidt-Mende, J.K. Stolarczyk, Angew. Chem. Int. Ed. 125 (2013) 7516–7557.
[4] G.B. Chen, R. Gao, Y.F. Zhao, Z.H. Li, G.I.N. Waterhouse, R. Shi, J.Q. Zhao, M.T. Zhang,
L. Shang, G.Y. Sheng, X.P. Zhang, X.D. Wen, L.Z. Wu, C.H. Tung, T.R. Zhang, Adv. Mater. 30 (2018) 3.
[5] R. Kuriki, K. Sekizawa, O. Ishitani, K. Maeda, Angew. Chemie Int. Ed. 54 (2015) 2406–2409.
[6] L.B. Hoch, T.E. Wood, P.G.G. O'Brien, K. Liao, L.M. Reyes, C.A. Mims, G.A. Ozin, Adv. Sci. 1 (2014) 1.
[7] T. Zhang, J.X. Low, X.X. Huang, J.F. Al-Sharab, J.G. Yu, T. Asefa, Chemcatchem 9 (2017) 3054–3062.
[8] J. Jin, J.G. Yu, D.P. Guo, C. Cui, W.K. Ho, Small 11 (2015) 5262–5271.
[9] A. Iwase, S. Yoshino, T. Takayama, Y.H. Ng, R. Amal, A. Kudo, J. Am. Chem. Soc. 138 (2016) 10260–10264.
[10] L. Liang, F.C. Lei, S. Gao, Y.F. Sun, X.C.Jiao.J. Wu, S. Qamar, Y. Xie, Angew. Chem. Int. Ed. 54 (2015) 13971–13974.
[11] Q. Kang, T. Wang, P. Li, L.Q. Liu, K. Chang, M. Li, J.H. Ye, Angew. Chem. 127 (2015) 855–859.
[12] D.R. Sun, Y.H. Gao, J.L. Fu, X.C. Zeng, Z.N. Chen, Z.H. Li, Chem. Commun. 51 (2015) 2645–2648.
[13] D.S. Chen, H.Z. Xing, C.G. Wang, Z.M. Su, J. Mater. Chem. A 4 (2016) 2657–2662.
[14] M.R. Hoffmann, S.T. Martin, W. Choi, D.W. Bahnemann, Chem. Rev. 95 (1995) 69–96.
[15] S.U.M. Khan, M. Al-Shahry, W.B. Ingler, Science 297 (2002) 2243–2245.
[16] X. Wu, Z.G. Chen, Q.L. Gao, L.Z. Wang, Adv. Funct. Mater. 21 (2011) 4167–4172.
[17] Y. Paz, Appl. Catal. B-Environ. 99 (2010) 448–460.
[18] Q.J. Xiang, J.G. Yu, M. Jaroniec, J. Am. Chem. Soc. 134 (2012) 6575–6578.
[19] T. Sun, J. Fan, E.Z. Liu, L.S. Liu, Y. Wang, H.Z. Dai, Y.H. Yang, W.Q. Hou, X.Y. Hu, Z.Y. Jiang, Powder Technol. 228 (2012) 210–218.
[20] E.Z. Liu, J. Fan, X.Y. Hu, Y. Hu, H. Li, C.N. Tang, L. Sun, J. Wan, J. Mater. Chem. 50 (2015) 2298–2305.
[21] Y.T. Li, L. Chen, Y.L. Guo, X.G. Sun, Y. Wei, Chem. Eng. J. 181 (2012) 734–739.
[22] S.S. Kalanur, H.L. Sun, J.H. Yun, O.S. Joo, J. Photochem. Photobiol. A 259 (2013) 1–9.
[23] Z. Bian, T. Tachikawa, W. Kim, W.Y. Choi, T. Majima, J. Phys. Chem. C 116 (2016) 25444–25453.
[24] S. Yanagida, M. Makino, T. Ogaki, A. Yasumori, J. Electrochem. Soc. 159 (2012) B845–B849.
[25] L.N. Han, H.Q. Li, S.J. Choi, M.S. Park, S.M. Lee, Y.J. Kim, D.W. Park, Appl. Catal. A-Gen. 429 (2012) 67–72.
[26] L. Sun, J. Li, C.L. Wang, S.F. Li, Y.K. Lai, H.B. Chen, C.J. Lin, J. Hazard. Mater. 171 (2009) 1045–1050.
[27] V. Houšková, V. Štengl, S. Bakardjieva, N. Murafa, V. Tyrpekl, Appl. Catal. B-Environ. 89 (2009) 613–619.
[28] J.G. Yu, J.X. Low, W. Xiao, P. Zhou, M. Jaroniec, J. Am. Chem. Soc. 136 (2014) 8839–8842.
[29] Y.P. Xie, G. Liu, L.C. Yin, H.M. Cheng, J. Mater. Chem. 22 (2012) 6746–6751.
[30] S.Q. Huang, Z.Y. Lou, Z.B. Qi, N.W. Zhu, H.P. Yuan, Appl. Catal. B-Environ. 168 (2015) 313–321.
[31] T. Ohnoa, T. Higoa, N. Murakami, H. Saitoa, Q. Zhanga, Y. Yanga, T. Tsubota, Appl. Catal. B-Environ. 152 (2014) 309–316.
[32] Q.Q. Lang, W.L. Hu, P.H. Zhou, T.L. Huang, S.X. Zhong, L.N. Yang, J.R. Chen, S. Bai, Nanotechnology 28 (2017) 484003.
[33] L.J. Liu, D.T. Pitts, H.L. Zhao, C.Y. Zhao, Y. Li, Appl. Catal. A-Gen. 467 (2013) 474–482.
[34] K. Li, T.Y. Peng, Z.H. Ying, S.S. Song, J. Zhang, Appl. Catal. B-Environ. 180 (2016) 130–138.
[35] Z.K. Zheng, B.B. Huang, X.Y. Qin, X.Y. Zhang, Y. Dai, M.H. Whangbo, J. Mater. Chem. 21 (2011) 9079–9087.
[36] Y. Xie, K.L. Ding, Z.M. Liu, R.T. Tao, Z.Y. Sun, H.Y. Zhang, G. An, J. Am. Chem. Soc. 131 (2009) 6648–6649.
[37] P. Wang, B.B. Huang, X.Y. Qin, X.Y. Zhang, Y. Dai, M.H. Whangbo, Inorg. Chem. 48 (2009) 10697–10702.
[38] Md.S.A.S. Shah, M. Nag, T. Kalagara, S. Singh, S.V. Manorama, Chem. Mater. 20 (2008) 2455–2460.
[39] Y. Kobayashi, V. Salgueiriño-Maceira, L.M. Liz-Marzán, Chem. Mater. 13 (2001) 1630–1633.
[40] P. Wang, B.B. Huang, Y. Dai, M.H. Whangbo, Phys. Chem. Chem. Phys. 14 (2012) 9813–9825.
[41] H.W. Huang, L.Y. Liu, Y.H. Zhang, N. Tian, RSC Adv. 5 (2015) 1161–1167.
[42] J. Ding, Z. Dai, F. Qin, H.P. Zhao, S. Zhao, R. Chen, Appl. Catal. B-Environ. 205 (2017) 281–291.
[43] J. Ding, Z. Dai, F. Tian, B. Zhou, B. Zhao, H.P. Zhao, Z.Q. Chen, Y.L. Liu, R. Chen, J. Mater. Chem. A 5 (2017) 23453–23459.
[44] K. Wang, Q. Li, B.S. Liu, B. Cheng, W.K. Ho, J.G. Yu, Appl. Catal. B-Environ. 176 (2015) 44–52.
[45] X.L. Zhu, X.Z. Liang, P. Wang, Y. Dai, B.B. Huang, Appl. Surf. Sci. 456 (2018) 493–500.
[46] X.Z. Liang, P. Wang, M.M. Li, Q.Q. Zhang, Z.Y. Wang, Y. Dai, X.Y. Zhang, Y.Y. Liu, M.H. Whangbo, B.B. Huang, Appl. Catal. B-Environ. 220 (2018) 356–361.
[47] X.L. Liu, X.Z. Liang, P. Wang, B.B. Huang, X.Y. Qin, X.Y. Zhang, Y. Dai, Appl. Catal. B-Environ. 203 (2017) 282–288.
[48] G.Z. Wang, Q.L. Sun, Y.Y. Liu, B.B. Huang, X.Y. Qin, X.Y. Zhang, Y. Dai, Chemistry 21 (2015) 2364–2367.
[49] R. Asahi, T. Morikawa, T. Ohwaki, K. Aoki, Y. Taga, Science 293 (2001) 269–271.
[50] Z.Z. Lou, B.B. Huang, X.Y. Qin, X.Y. Zhang, Z.Y. Wang, Z.K. Zheng, H.F. Cheng, Y. Dai, Crystengcomm. 13 (2011) 1789–1793.
[51] Z.K. Zheng, B.B. Huang, Z.Y. Wang, M. Guo, P. Wang, X.Y. Qin, X.Y. Zhang, Y. Dai, J. Phys. Chem. C 113 (2009) 462–470.
[52] S.C. Parker, P.M. Oliver, N.H.D. Leeuw, J.O. Titiloye, G.W. Watson, Phase. Transit. 61 (1997) 83–107.
[53] X.Q. Gong, A. Selloni, Appl. Catal. B-Environ. 109 (2005) 19560–19562.
[54] N.Q. Wu, J. Wang, D.N. Tafen, H. Wang, J.G. Zheng, J.P. Lewis, X.G. Liu, S.S. Leonard, A. Manivannan, J. Am. Chem. Soc. 132 (2010) 6679–6685.
[55] M. Hashim, C.G. Hu, X. Wang, B.Y. Wan, J. Xu, Mater. Res. Bull. 47 (2012) 3383–3389.
[56] L.A. Peyser, A.E. Vinson, A.P. Bartko, R.M. Dickson, Science 291 (2001) 103–106.